Available online at www.sciencedirect.com

SciVerse ScienceDirect

Ceramics International 38 (2012) 6151–6156

CERAMICS INTERNATIONAL

www.elsevier.com/locate/ceramint

Mechanical properties of sintered $La_{9.33}Si_2Ge_4O_{26}$ oxyapatite materials for SOFC electrolytes

M. Santos[a], C. Alves[b], F.A.C. Oliveira[b], T. Marcelo[b], J. Mascarenhas[b], J.V. Fernandes[a], B. Trindade[a,*]

[a]*CEMUC, Mechanical Engineering Department, University of Coimbra, Rua Luís Reis Santos, Coimbra 3030-788, Portugal*
[b]*Laboratório Nacional de Energia e Geologia I.P., Estrada do Paço do Lumiar, Lisboa 1649-038, Portugal*

Received 3 April 2012; received in revised form 26 April 2012; accepted 26 April 2012
Available online 5 May 2012

Abstract

Mechanical properties of $La_{9.33}Si_2Ge_4O_{26}$ prepared by mechanical alloying and subsequent sintering at 1300–1400 °C for 1 h were evaluated. Hardness and Young's modulus values in the range 7.3–9.6 GPa and 106–135 GPa, respectively, were obtained from nanohardness tests. The fracture toughness values derived from the Palmqvist method varied between 3.5 and 3.9 MPa $m^{1/2}$ from classical microindentation test with an indentation load of 9.8 N. Yield stress (σ_y) was determined by inverse analysis from microhardness tests. The maximum value of σ_y (1829 MPa) was obtained for the sample sintered at 1400 °C showing the highest density (5.42 g/cm^3).

Keywords: C. Mechanical properties; Lanthanum-based oxyapatite; Mechanical alloying; SOFC

1. Introduction

M-doped lanthanum oxides of general formula $La_{10}(MO_4)_6O_2$ where M is an element such as Ge, Si, Al, are being considered for a range of technological applications, such as electrolytes in solid oxide fuel cells (SOFCs). These materials have been obtained by different techniques, such as solid state reaction [1], sol–gel synthesis [2], hot-pressing [3], mechanical milling [4], precipitation combined with an azeotropic-distillation process [5], colloidal processing [6] and floating zone methods [7]. All these processes require high temperature consolidation or heat treatment processes in order to obtain dense materials with apatite-type structure, with suitable high ion conductivity. In addition, these materials must be chemically stable and possess adequate mechanical properties such as high hardness, rigidity and fracture toughness in order to assure a desirable performance of the anode-electrolyte-cathode final assembly.

In a recent study [8], powders of La_2O_3, SiO_2 and GeO_2 were used to obtain $La_{9.33}Si_2Ge_4O_{26}$ materials with an apatite-type structure. Mechanical alloying was used as synthesis technique for obtaining the desired structure with doping Ge atoms in the tetrahedral sites of the apatite phase. The mechanically alloyed powders were subsequently consolidated at lower temperatures than those mentioned in the literature (1500–1600 °C). Dense samples were obtained at sintering temperatures of 1400 °C.

The present study evaluates the mechanical properties of $La_{9.33}Si_2Ge_4O_{26}$ samples obtained under different conditions of mechanical alloying and subsequent sintering. For this purpose, depth-sensing indentation techniques were used to evaluate hardness (H), Young's modulus (E), yield stress (σ_y) and fracture toughness (K_c) of the sintered samples.

2. Experimental

2.1. Sample preparation

Oxyapatite-based $La_{9.33}Si_2Ge_4O_{26}$ electrolytes have been prepared in a previous work [8] by conventional

*Corresponding author. Tel.: +351 239790794.
E-mail address: bruno.trindade@dem.uc.pt (B. Trindade).

0272-8842/$36.00
http://dx.doi.org/10.1016/j.ceramint.2012.04.065

Table 1
Experimental conditions used for materials fabrication and correspondent densification results.

Sample identification	Pre-milling time (min)	MA atmosphere	Compaction/pressure (MPa)	Sintering temperature (°C)	Sintering density (g/cm^3)	Open porosity (%)
S1	30	Argon	Uniaxial/393	1300	4.81	13.40
S2	30	Argon	Uniaxial/393	1350	5.13	6.15
S3	30	Argon	Uniaxial/393	1400	5.42	1.11
S4	0	Air	CIP/300	1400	5.13	4.18
S5	30	Air	Uniaxial/620	1400	5.36	1.80
S6	10	Air	Uniaxial/620	1400	5.34	2.36

pressureless sintering in an electrical furnace (SATER, SF8, Spain) from La_2O_3, SiO_2 and GeO_2 powders, milled at 350 rpm for 15 h, under controlled environmental conditions (Table 1). Some batches were prepared after pre-milling the starting materials. The powder mixtures were compacted either by cold isostatic pressing (CIP) or uniaxial pressing before sintering. The objective was to study the influence of pre-milling the raw powders and mixing them in different atmospheres (either Ar or air) on the densification behavior of MA powders at moderate temperatures (up to 1400 °C). The sintered samples consisted mainly of apatite and presented different sintered density as a function of the mechanical alloying (MA) and sintering conditions.

2.2. Mechanical characterization

The mechanical properties, including hardness, Young's modulus, yield stress and fracture toughness, of the samples were determined by the depth-sensing indentation technique and by conventional microindentation tests.

2.2.1. Nanoindentation tests

Nanoindentation tests were performed on polished surfaces using a NanoTest Platform from MicroMaterials, equipped with a Berkovich indenter. Corrections of the geometrical imperfections of the tip of the indenter, thermal drift of the equipment and zero indentation-depth position were performed. A 50 mN maximum load was used for the determination of hardness (H) and Young's modulus (E) according to the method described elsewhere [9]. In order to have representative average values for the evaluated properties, 100 indentation tests were performed on each sample.

In each test, the load was applied until the nominal load of 50 mN was reached, using a depth rate of 1.67 mN s^{-1}. Two creep periods of 30 s were programmed during the tests: at the maximum load, in order to stabilize the penetration depth before unloading, and during unloading, for thermal drift correction.

Hardness, H, is defined as the ratio between the maximum applied load during the indentation test, P_{max}, and the contact area of the indentation immediately before unloading, A_C [10]:

$$H = \frac{P_{max}}{A_c} \tag{1}$$

The following equation was used for determining the reduced Young's modulus, E_r [10]:

$$E_r = \frac{1}{2}\sqrt{\frac{\pi}{A_c}}\frac{1}{C-C_f} \tag{2}$$

where C is the compliance of the unloading part of the indentation curve ($C=(dh/dP)h_{max}$) and C_f is the frame compliance. In this equation, E_r is a function of the Young's modulus, E, and the Poisson's ratio, v, of the sample (s) and the indenter (i), through:

$$\frac{1}{E_r} = \frac{1-v_s^2}{E_s} + \frac{1-v_i^2}{E_i} \tag{3}$$

The so-called reduced elastic modulus of the material, E^*, is such that:

$$\frac{1}{E^*} = \frac{1-v_s^2}{E_s} \tag{4}$$

For evaluation of the hardness (Eq. (1)) and Young's modulus (Eqs. (2) and (3)), a Berkovich indenter was used and it was assumed that the contact penetration depth, h_c, and consequently the contact area A_C ($A_C = 24.5h^2$ in an ideal case) immediately before unloading, was directly determined from the load–unloading curve, as follows:

$$h_C = h_{max} - \varepsilon C P_{max} \tag{5}$$

where h_{max} is the indentation depth corresponding to the maximum load, P_{max}, and ε is a correction factor, which depends on the indenter geometry (for the Berkovich indenter, $\varepsilon = 0.75$ was used [10]).

2.2.2. Microindentation tests

A Shimatzu indentation equipment with a Vickers diamond indenter was used for the determination of Vickers hardness ($HV1$) and fracture toughness (K_c). The $HV1$ values were converted in GPa for comparison with the hardness measured by the depth sensing indentation technique. The fracture toughness (K_c) was determined by applying the Palmqvist method [11]. In this method, the value of K_c is obtained from the measurement of the length of cracks arising from the corners of hardness indentations, using the

equation:

$$K_c = 0.087\sqrt{HW} \quad (6)$$

where $W = P/L_T$, being P the applied nominal load, and L_T the total length of cracks. The total crack length formed on the four corners of the diamond indenter was measured using an optical microscope (Zeiss, Jenaphot 2000) at 400× magnification. A 9.8 N load was chosen for the indentation tests. Ten measurements from randomly selected areas of each sample were performed for analysis, according to the ASTM standard E384-99 [12].

In order to better define the mechanical behavior of the samples, namely the overall level of the stress (σ) – plastic strain (ε) curves, two reverse analysis methodologies [13,14] were employed. Both σ and ε can be derived using the swift equation, which has been successfully used in continuum plastic theory (see for example [15]):

$$\sigma = k(\varepsilon + \varepsilon_0)^n \quad (7)$$

where k, ε_0 and n are constants of the material, such that $\sigma_y = k\varepsilon_0^n$, where σ_y is the yield stress.

These reverse analysis approaches were carried out making use of the experimental micro-indentation results to estimate the representative stress (σ_r—the flow stress corresponding to a plastic strain value – representative plastic strain ε_r – in the range 3.3%–4.2%, depending on the Young's modulus and representative stress values [14]). Both approaches are based on the fact that materials with the same reduced elastic modulus, E^*, and representative stress, σ_r, exhibit similar behavior under loading indentation, whatever the value of the strain-hardening exponent, n.

In the case of the reverse analysis approach proposed by Dao et al. [14], an analytical method is used to determine σ_r (corresponding to a plastic strain value ε_r of 3.3%), which consists of using a dimensionless function Π_1:

$$\Pi_1 = \frac{K}{\sigma_r} = -1.131\left[ln\left(\frac{E^*}{\sigma_r}\right)\right]^3 + 13.635\left[ln\left(\frac{E^*}{\sigma_r}\right)\right]^2 - 30.594\left[ln\left(\frac{E^*}{\sigma_r}\right)\right] + 29.267 \quad (8)$$

where K is the curvature of the loading part of the load–indentation depth curve, in agreement with Kick's law:

$$P = Kh^2 \quad (9)$$

where P and h are the load and indentation depth, respectively. The use of Eq. (8), for estimation of the representative stress, σ_r, presumes the previous experimental determination of the reduced elastic modulus of the material, E^* (obtained by nanoindentation), and the K parameter, which can be obtained from the microhardness tests from the knowledge of the pair (P_{max}, h_{max}).

The reverse analysis approach proposed by Antunes et al. [13] directly compares experimental to numerical simulation indentation results. This reverse analysis methodology extracts the representative stress, σ_r, by comparing the loading part of the experimental and numerical indentation curves (in the case of conventional microhardness results the comparison can be made at the maximum load). In the current investigation, representative plastic strain values ε_r equal to 3.5% were found for the materials studied.

A quasi-linear relationship between E^*/H and E^*/σ_r was observed [13], independent of the work-hardening coefficient:

$$\frac{E^*}{H} = 0.231\left(\frac{E^*}{\sigma_r}\right) + 4.910 \quad (10)$$

The use of this equation, to estimate the representative stress, σ_r, presumes that the hardness, H, and the reduced elastic modulus, E^* (obtained by nanoindentation), of the material, have previously been determined. The representative stress obtained from this equation can still be optimized by comparing the experimental nominal applied load with the load attained at the same indentation depth in the numerical indentation curves. The value of the representative stress, in the numerical iterations, is altered until the numerical curve coincides with the experimental curve.

The yield stress, σ_y, of the samples was estimated from Eq. (7) considering a value of strain hardening coefficient, n, of 0.02. This low value is consistent with brittle ceramics, such as the apatite under study.

3. Results and discussion

Fig. 1 shows a typical example of a load (P) vs. indentation depth (h) curve obtained from sintered sample S4, similar to the ones obtained for the other samples. These curves have, in general, a regular feature resulting from a good surface finishing. Based on these curves, nanohardness and Young's modulus values were calculated for all the sintered samples (Table 2).

Very similar values of H were determined for the sintered samples, independently of the manufacturing parameters. The lowest value ($H = 7.3$ GPa) was obtained for sample S4, which was fabricated directly from the initial powders (without pre-milling), compacted by CIP at

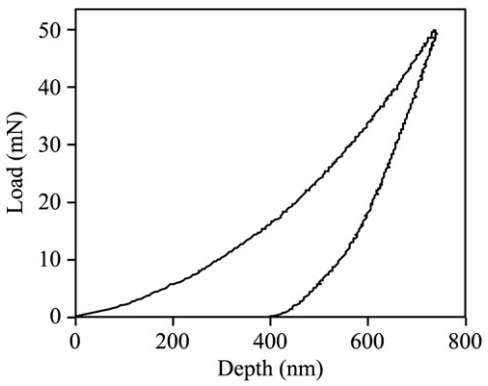

Fig. 1. Load–depth indentation curve from sample S4.

Table 2
Nanohardness (H) and Young's modulus (E) of the sintered samples.

Sample	H (GPa)	E (GPa)
S1	8.5 ± 1.1	123 ± 8
S2	8.5 ± 1.4	130 ± 11
S3	9.8 ± 1.3	121 ± 9
S4	7.3 ± 1.3	106 ± 8
S5	9.6 ± 1.2	135 ± 8
S6	9.2 ± 1.4	117 ± 10

300 MPa and presssureless sintered at 1400 °C. This sample presents a sintered density of 5.13 g/cm^3 and an open porosity of 4.2%. Considering the range of density and open porosity values obtained for all samples, one can observe that those values fall within the middle of the range. Therefore, this lower H value of sample S4 appears to be related to structural features rather than to porosity alone. In fact, the applied load (50 mN) was relatively low, which minimizes the influence of porosity on the measurements. Indeed, one can see that the results obtained from samples S1 and S2, which have very different densities and porosities, show similar values of H.

To the author's knowledge, scarce data on hardness exist in the literature for this type of lanthanum silicates. Mukherjee et al. [16] in a comparative study of "gels" and oxide mixtures as starting materials for the nucleation and crystallization of silicate glasses (SiO_2-rich), measured the hardness of samples with different SiO_2–La_2O_3 compositions. The values obtained were around 6.5 GPa for an applied load of 0.98 N. The values obtained in this work with a much lower load (50 mN) are higher than 6.5 GPa, which is in agreement with the well known dependence of the hardness on the applied load. Vullo et al. [17] reported a value of 650HK (Knoop hardness with 0.981 N load) for lanthanum silicates-based materials.

Concerning Young's modulus, the values obtained are in the range 106–135 GPa, the sample with the lowest H (7.3 GPa) being the one with the lowest value of E (106 GPa). These values are in good agreement with those available in the literature. Indeed, according to Vullo et al. [17], lanthanum silicates are known for their high elastic constants, exhibiting high Young's modulus ($E \approx 100$ GPa) when compared to other silicate type materials. These values are, however, lower than the ones reported for other materials used in SOFC's. For instance, a value of 220 GPa is typical of a fully dense zirconia-based material stabilized with 8% mol of Y_2O_3 [18].

Table 3 compiles $HV1$ and K_C results obtained from the sintered samples. The $HV1$ values were converted to GPa for comparison with the hardness measured by the depth sensing indentation technique (Table 2). Fig. 2 shows a SEM observation of a Vickers indentation from sample S3, in which cracks at the corners of the indentation are evident. The H values obtained varied in the range of 2.9 to 5.8 GPa and as expected they are significantly lower

Table 3
Vickers microhardness ($HV1$) and fracture toughness (K_c) of the sintered samples.

Sample	H $HV1$/(GPa)	K_c (MPa m$^{1/2}$)
S1	279/2.9	3.5
S2	407/4.3	3.8
S3	541/5.7	3.9
S4	448/4.7	3.5
S5	550/5.8	3.8
S6	523/5.5	3.7

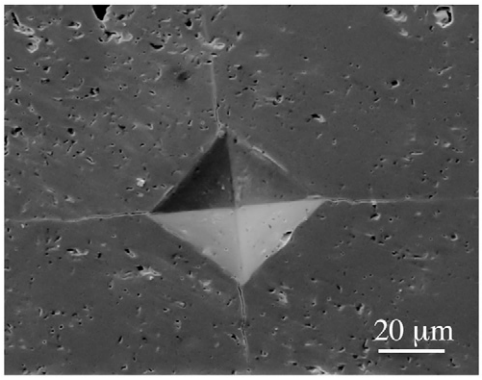

Fig. 2. Cracks at the corners of a Vickers indentation from sample S3 (P=9.8 N).

than the ones obtained with a load of 50 mN. This is a well-known phenomenon, which has been also reported for other ceramic materials. In fact, Roa et al. [19] used microindentation and nanoindentation tests with different applied loads for the determination of hardness and Young's modulus of lanthanum tungstates. They observed an indentation size effect, i.e. a significant dependence of hardness on the applied load (apparent hardness values in the range 7.5 to 14.5 GPa were obtained). Contrarily, the Young's modulus did not vary significantly with penetration depth, as expected.

A clear dependence of the $HV1$ hardness on the porosity level of the sintered samples was observed, as shown in Fig. 3. The higher the porosity level, the lower the hardness (quite evident for porosity levels higher than 2%—samples S1, S2 and S4).

The values of fracture toughness obtained are in the range 3.5–3.9 MPa m$^{1/2}$. Although the differences are not significant, the higher K_c values are associated to less porous samples (S3, S5 and S6). According to Shaobo et al. [20] and Smith et al. [21], indentation toughness based on median crack models can deviate from conventional four-point bending toughness values by up to 30% in single phase ceramics and glasses. This suggests that the K_{IC} of the $La_{9.33}Si_2Ge_4O_{26}$ apatite phase might reach the value of 5 MPa m$^{1/2}$ (30% higher than 3.9 MPa m$^{1/2}$).

Table 4 shows the σ_y and σ_r values of samples S1 to S6 obtained from the two reverse analysis methodologies used

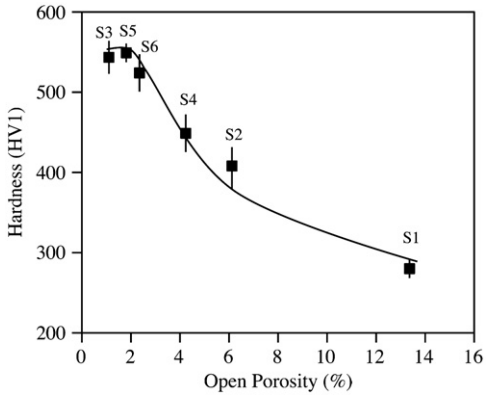

Fig. 3. Influence of open porosity on *HV1* hardness for the sintered samples.

Table 4
σ_y and σ_r values of the samples obtained from two reverse analysis methods.

Sample	Antunes et al. [13]		Dao et al. [14]	
	σ_y (MPa)	σ_r (MPa)	σ_y (MPa)	σ_r (MPa)
S1	779	812	771	804
S2	1169	1219	1185	1235
S3	1829	1907	1720	1793
S4	1467	1529	1410	1470
S5	1759	1834	1712	1785
S6	1781	1856	1665	1736

[13,14]. The values obtained from these methods do not differ significantly. For both methods, the σ_y values are slightly lower than the σ_r ones, as a result of the low coefficient n used in the calculations. Nevertheless, different values were obtained for samples S1 to S6. The σ_y values obtained are in the range 779–1829 MPa using the Antunes et al. [13] methodology and 771–1720 MPa when using the Dao et al. [14] one. In both cases, the lowest value corresponds to sample S1, sintered at the lowest temperature, with the lowest hardness and the highest open porosity. Sample S3 shows the highest value of σ_y (1829 or 1720 GPa, depending on the methodology used). This sample was sintered at 1400 °C, with a final porosity of 1.1% (the lowest value measured).

4. Conclusions

The mechanical properties of $La_{9.33}Si_2Ge_4O_{26}$ samples obtained by mechanical alloying and subsequent sintering were evaluated by the depth-sensing indentation technique and by conventional microindentation tests.

The results show that the mechanical properties are significantly influenced by the sintering temperature. Hardness values and Young's modulus in the ranges 7.3–9.6 GPa and 106–135 GPa, respectively, were obtained from nanohardness tests. As expected, significant lower values of hardness (2.9–5.8 GPa) were obtained by conventional microindentation with a load of 9.8 N. The fracture toughness values did not show significant variation with the sintering temperature the results ranging from 3.5 to 3.9 MPa $m^{1/2}$. The maximum value of σ_y (1829 MPa) was obtained for samples showing the highest density (5.42 g/cm^3).

Acknowledgments

This research is partially sponsored by FEDER funds through the program COMPETE – Programa Operacional Factores de Competitividade – and by national funds through FCT – Fundação para a Ciência e a Tecnologia – under the project PTDC/EME-PME/102837/2008. The research fellowships granted to Cátia Alves and Márcio Santos are also gratefully acknowledged.

References

[1] Y. Higuchi, M Sugawara, K. Onishi, M. Sakamoto, S. Nakayama, Oxide ionic conductivities of apatite-type lanthanum silicates and germanates and their possibilities as electrolyte of lower temperature operating SOFC, Ceramics International 36 (2010) 955–959.
[2] E. Jothinathan, K Vanmeensel, J. Vleugels, O. Van der Biest, Powder synthesis, processing and characterization of lanthanum silicates for SOFC applications, Journal of Alloys and Compounds 495 (2010) 552–555.
[3] P.J. Panteix, I Julien, D. Bernache-Assollant, P. Abélard, Synthesis and characterization of oxide ions conductors with the apatite structure for intermediate temperature SOFC, Materials Chemistry and Physics 95 (2006) 313–320.
[4] L.G. Martínez-González, E Rodrigue Reina, K.J. Moreno, J.I. Escalante-García, A.F. Fuentes, Ionic conductivity of apatite-type rare-earth silicates prepared by mechanical milling, Journal of Alloys and Compounds 476 (2009) 710–714.
[5] H.C. Yao, J.S Wang, G.G. Hu, J.F. Li, X.R. Lu, Z.J. Li, New approach to develop dense lanthanum silicate oxyapatite sintered ceramics with high conductivity, Solid State Ionics 181 (2010) 41–47.
[6] I. Santacruz, J.M Porras-Vázquez., E.R. Losilla, M.I. Nieto, R. Moreno, M.A.G. Aranda, Preparation of aluminium lanthanum oxyapatite tapes, $La_{10}AlSi_5O_{26.5}$, by tape casting and reaction sintering, Journal of the European Ceramic Society 31 (2011) 1573–1580.
[7] S. Nakayama, M Sakamoto, M. Higuchi, K. Kodaira, M. Sato, S. Kakita, T. Suzuki, K. Itoh, Oxide ionic conductivity of apatite type $Nd_{9.33}(SiO_4)6O_2$ single crystal, Journal of the European Ceramic Society 19 (1999) 507–510.
[8] R. Serra, C.Alves, F.A.C. Oliveira, T. Marcelo, J. Mascarenhas, B. Trindade, Enhanced sinterability of mechanical alloyed $La_{9.33}Si_2Ge_4O_{26}$ oxyapatite powders for IT-SOFC electrolytes. Accepted for Publication in Ceramics International. http://dx.doi.org/10.1016/j.ceramint.2012.03.042.
[9] A. Sakly, J. Costa, B. Trindade, J.V. Fernandes, T. Benameur, Nanostructured Mo_3Al-based composites strengthened by Al_2O_3 precipitates, Journal of Alloys and Compounds 502 (2010) 480–487.
[10] J.M. Antunes, A. Cavaleiro, L.F. Menezes, M.I. Simões, J.V. Fernandes, Ultra-microhardness testing procedure with Vickers indenter, Surface and Coatings Technology 149 (2002) 27–35.
[11] R. Spiegler, S. Schmaddler, L.S. Sigl, Fracture toughness evaluation of WC-Co alloys by indentation testing, Journal of Hard Materials 1 (1990) 147–158.
[12] ASTM E384-99 Standard test method for microindentation hardness of materials, ASTM International, West Conshohocken, PA, USA, 1999.

[13] J.M. Antunes, J.V. Fernandes, L.F Menezes, B.M. Chaparro, A new aproach for reverse analyses in depth-sensing indentation using numerical simulation, Acta Materialia 55 (2007) 69–81.
[14] M. Dao, N. Chollacoop, K.J. Vliet, T.A. Venkatesh, S. Suresh, Computational modeling of the forward and reverse problems in instrumented sharp indentation, Acta Materialia 49 (2001) 3899–3918.
[15] J.V. Fernandes, D.M. Rodrigues, L.F. Menezes, M.F. Vieira, A modified swift law for prestrained materials, International Journal of Plasticity 14 (1998) 537–550.
[16] S.P. Mukherjee, J. Zarzycki, J.P. Traverse, Influence of hydroxyl groups on the crystallization of lanthanum silicate glass, Journal of Non-Crystalline Solids 20 (1976) 455–458.
[17] P. Vullo, M.J. Davis, Comparative study of micro-indentation and Chevron notch fracture toughness measurements of silicate and phosphate glasses, Journal of Non-Crystalline Solids 349 (2004) 180–184.
[18] S. Giraud, J. Canel, Young's modulus of some SOFCs materials as a function of temperature, Journal of the European Ceramic Society 28 (1) (2008) 77–83.
[19] J.J. Roa, A. Magraso, M. Morales, P. Núnez, M. Segarra, Determination of hardness, Young's modulus and fracture toughness of lanthanum tungstates as novel proton conductors, Ceramics International 37 (2011) 1593–1599.
[20] X. Shaobo, L. Guangxia, L. Changchun, Application of Indentation Technique in Determining Fracture Toughness of Ceramics, Engineering Fracture Mechanics 31 (1988) 309–313.
[21] S.S. Smith, P. Magnusen, B.J. Pletka, Fracture mechanics methods for ceramics, rocks and concrete, ASTM STP 745, American Society for Testing and Materials, Philadelphia, PA, 1981 33–45.